

Strong-Coupling and the Stripe Phase of ^3He

Joshua J. Wiman¹ · J. A. Sauls¹

Received: 3 May 2016 / Accepted: 23 May 2016 / Published online: 3 June 2016
© Springer Science+Business Media New York 2016

Abstract Thin films of superfluid ^3He were predicted, based on weak-coupling BCS theory, to have a stable phase which spontaneously breaks translational symmetry in the plane of the film. This crystalline superfluid, or “stripe” phase, develops as a one-dimensional periodic array of domain walls separating degenerate B phase domains. We report calculations of the phases and phase diagram for superfluid ^3He in thin films using a strong-coupling Ginzburg–Landau theory that accurately reproduces the bulk ^3He superfluid phase diagram. We find that the stability of the Stripe phase is diminished relative to the A phase, but the Stripe phase is stable in a large range of temperatures, pressures, confinement, and surface conditions.

Keywords Superfluid ^3He · Phase transitions · Confined quantum liquids

1 Introduction

The theoretical prediction of a crystalline superfluid, or “stripe” phase, that spontaneously breaks translational symmetry in thin films of ^3He [1], along with advances in nanoscale fabrication and experimental instrumentation [2], has renewed interest in the properties of superfluid ^3He in thin films and confined geometries. Recent theoretical work on nanoscale cylindrical channels predict several new phases of ^3He not realized in bulk ^3He , including the polar phase, two distinct chiral phases with different symmetries, and a periodic domain wall phase that spontaneously breaks translational

✉ Joshua J. Wiman
jjwiman@u.northwestern.edu

J. A. Sauls
sauls@northwestern.edu

¹ Department of Physics & Astronomy, Northwestern University, Evanston, IL, USA

symmetry along the axis of the channel, and is analogous to the predicted Stripe phase in thin films [3,4]. Experiments to search for these new phases in 100 nm cylindrical channels are in progress.¹ In an exciting development, recent reports of NMR experiments on ³He confined within anisotropic aerogels identify NMR signatures for the superfluid polar phase [5]. This phase appears to be ideally suited for stabilizing half-quantum vortices [6]. The combination of disorder and confinement has also led to new realizations of Larkin–Imry–Ma phases [5,7]. Recently, experiments on superfluid ³He under planar confinement have been done on individual, precisely fabricated slabs, in part to search for the Stripe phase [2]. In the weak-coupling limit of BCS theory the Stripe phase is predicted to be stable in a large region of temperature and pressure for films of thickness $D \sim 700$ nm. However, the recent experiments on ³He confined in slabs of thickness $D \approx 700$ nm and $D \approx 1080$ nm have failed to detect the evidence of the Stripe phase [2].

A limitation of the Vorontsov and Sauls theory is that it does not include strong-coupling corrections to the BCS free energy. In bulk ³He, weak-coupling theory predicts a stable B phase at all temperatures and pressures; however, the A phase is found to be stable experimentally at T_c and pressures above $p_{PCP} \approx 21.22$ bar, with a first-order transition at $T_{AB} < T_c$ to the B phase. Theoretically, accounting for the stability of the A phase requires including next-to-leading order corrections to the full free energy functional, i.e., corrections to the weak-coupling functional [8]. While these strong-coupling corrections are largest at high pressures, they remain significant even for $p \sim 0$ bar [9]. Thus, for superfluid ³He confined within a film, it is to be expected that strong-coupling effects will increase the stability of the A phase relative to both the B- and Stripe phases, which could diminish, or even eliminate, the experimentally accessible region of the Stripe phase.

In this paper, we report our study of the A-Stripe and Stripe-B superfluid transitions using a Ginzburg–Landau (GL) functional that incorporates strong-coupling corrections to the weak-coupling GL material coefficients and accurately reproduces the bulk superfluid ³He phase diagram [3]. Within this strong-coupling GL theory, we calculate the superfluid order parameter and phase diagram as a function of pressure, temperature, confinement, and surface conditions.

2 Ginzburg–Landau Theory

The general form of the p-wave, spin triplet order parameter for ³He is given by the mean-field pairing self energy, which can be expanded in the basis of symmetric Pauli matrices ($S = 1$) and vector basis of orbital momenta ($L = 1$),

$$\hat{\Delta}(\hat{p}) = \sum_{\alpha i} A_{\alpha i} (i\sigma_{\alpha}\sigma_y) \hat{p}_i, \quad (1)$$

where \hat{p} is the direction of relative momentum of the Cooper pairs defined on the Fermi surface, and $A_{\alpha i}$ are the elements of a 3×3 complex matrix,

¹ W. P. Halperin, private communication.

$$A = \begin{pmatrix} A_{xx} & A_{xy} & A_{xz} \\ A_{yx} & A_{yy} & A_{yz} \\ A_{zx} & A_{zy} & A_{zz} \end{pmatrix}, \quad (2)$$

that transforms as a vector under spin rotations (with respect to α) and (separately) as a vector under orbital rotations (with respect to i). We choose aligned spin and orbital coordinate axes.

2.1 Free Energy Functional

To determine the order parameter and the phase diagram of ^3He in a film geometry, we solve the Euler–Lagrange equations of the GL functional, subject to relevant boundary conditions, and calculate the order parameter and the stationary free energy. The GL functional is defined by bulk and gradient energies with temperature-dependent strong-coupling corrections, and is supplemented by boundary conditions that we can tune from maximal to minimal pairbreaking [3].

The GL free energy functional is expressed in terms of invariants constructed from the order parameter matrix, A , and is given by [10]

$$\begin{aligned} \Omega[A] = \int_V d\mathbf{R} \left\{ \alpha(T) \text{Tr} (AA^\dagger) + \beta_1 \left| \text{Tr} (AA^T) \right|^2 + \beta_2 \left[\text{Tr} (AA^\dagger) \right]^2 \right. \\ + \beta_3 \text{Tr} \left[AA^T (AA^T)^* \right] + \beta_4 \text{Tr} \left[(AA^\dagger)^2 \right] + \beta_5 \text{Tr} \left[AA^\dagger (AA^\dagger)^* \right] \\ \left. + K_1 \left(\nabla_k A_{\alpha j} \nabla_k A_{\alpha j}^* \right) + K_2 \left(\nabla_j A_{\alpha j} \nabla_k A_{\alpha k}^* \right) + K_3 \left(\nabla_k A_{\alpha j} \nabla_j A_{\alpha k}^* \right) \right\}. \quad (3) \end{aligned}$$

In the weak-coupling limit, the GL material parameters are given by

$$\alpha^{\text{wc}}(T) = \frac{1}{3} N(0) (T/T_c - 1), \quad (4)$$

$$2\beta_1^{\text{wc}} = -\beta_2^{\text{wc}} = -\beta_3^{\text{wc}} = -\beta_4^{\text{wc}} = \beta_5^{\text{wc}}, \quad (5)$$

$$\beta_1^{\text{wc}} = -\frac{N(0)}{(\pi k_B T_c)^2} \left\{ \frac{1}{30} \left[\frac{7}{8} \zeta(3) \right] \right\}, \quad (6)$$

$$K_1^{\text{wc}} = K_2^{\text{wc}} = K_3^{\text{wc}} = \frac{7\zeta(3)}{60} N(0) \xi_0^2, \quad (7)$$

and determined by the normal-state, single-spin density of states at the Fermi energy, $N(0)$, the bulk transition temperature, T_c , and the Fermi velocity, v_f . The Cooper pair correlation length $\xi_0 \equiv \hbar v_f / 2\pi k_B T_c$ varies from $\xi_0 \simeq 770 \text{ \AA}$ at $p = 0$ bar to $\xi_0 \simeq 160 \text{ \AA}$ at $p = 34$ bar.

2.2 Strong-Coupling Corrections

The fourth-order β parameters that enter the GL free energy functional are modified by next-to-leading order corrections to the full Luttinger–Ward free energy functional

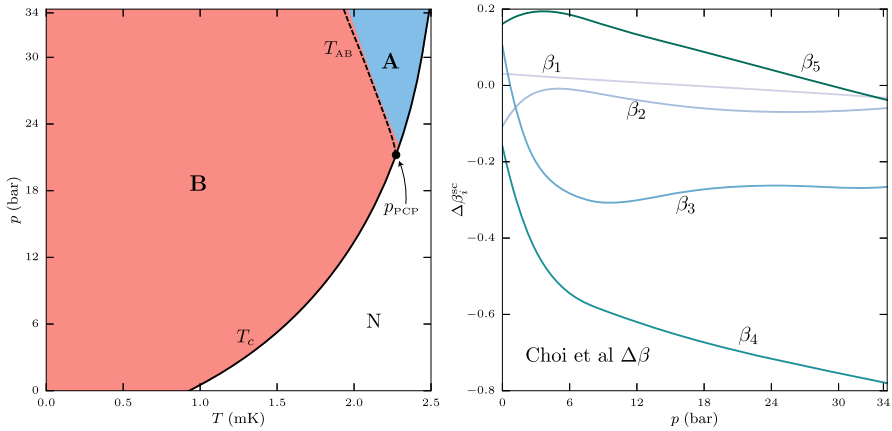


Fig. 1 *Left* Bulk phase diagram with *lines* showing the measured phase transitions and *shading* showing the calculated regions of phase stability based on GL theory. The $\Delta\beta_i^{\text{sc}}$ coefficients are from Choi et al. [9] and are plotted in the *right panel* (Color figure online)

[8]. These corrections scale as $\Delta\beta_i^{\text{sc}} \sim \beta_i^{\text{wc}}(T/T_F)$ near T_c . Combining the $\Delta\beta_i^{\text{sc}}$ with the weak-coupling coefficients in the bulk GL functional yields the critical pressure, p_{PCP} , above which the A phase is stable relative to the B phase. For $p > p_{\text{PCP}}$ the temperature scaling of the strong-coupling corrections relative to the weak-coupling β parameters breaks the degeneracy in temperature between the A and B phases at the critical pressure and accounts for the pressure dependence of the A–B transition line, $T_{\text{AB}}(p)$, and thus an accurate bulk phase diagram [3]. The resulting strong-coupling β parameters are given by

$$\beta_i(T, p) = \beta_i^{\text{wc}}(p, T_c(p)) + \frac{T}{T_c} \Delta\beta_i^{\text{sc}}(p). \tag{8}$$

Figure 1 shows the experimental bulk superfluid phase diagram as well as the phase diagram calculated from strong-coupling GL theory using $\Delta\beta_i^{\text{sc}}$ coefficients obtained based on analysis of selected experiments by Choi et al. [9] These β coefficients differ substantially from those calculated from strong-coupling theory based on a quasi-particle scattering amplitude that accounts for the normal Fermi liquid properties of ^3He . Figure 2 shows the bulk phase diagram calculated using the $\Delta\beta_i^{\text{sc}}$ from Sauls and Serene [11]. This set of β coefficients has a higher polycritical pressure than experiment; however, the pressure dependence of the $\Delta\beta_i^{\text{sc}}$ represents the expectation based on strong-coupling theory dominated scattering from ferromagnetic spin-fluctuations. Below $p = 12$ bar, the $\Delta\beta_i^{\text{sc}}$ are extrapolated to zero at a negative pressure corresponding to $T_c = 0$ [3].

2.3 Boundary Conditions

Confinement is represented in the GL theory through boundary conditions. For infinite, planar surfaces there are two limiting cases: maximal pairbreaking, due to the retro-re-

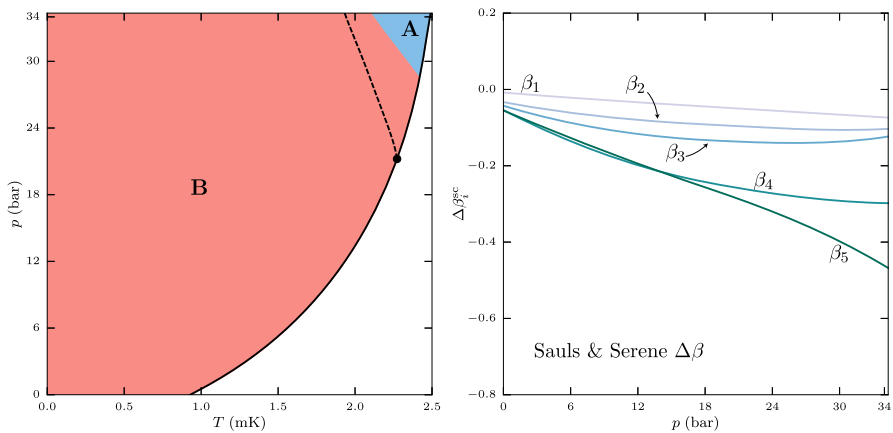


Fig. 2 Left Bulk phase diagram where the shaded regions represents the phases calculated from GL theory with the $\Delta\beta_i^{sc}$ of Sauls and Serene [11]. These strong-coupling corrections are plotted in the right panel (Color figure online)

flection of quasiparticles [12], and minimal pairbreaking, corresponding to specular reflection [13]. For a surface on the x - y plane with ^3He filling $z > 0$, maximal pairbreaking is defined within GL theory by

$$A_{\alpha i} \Big|_{z=0} = 0 \quad \forall i \in \{x, y, z\}, \tag{9}$$

while minimal pairbreaking is defined by

$$\begin{aligned} A_{\alpha z} \Big|_{z=0} &= 0, \\ \nabla_z A_{\alpha x} \Big|_{z=0} &= \nabla_z A_{\alpha y} \Big|_{z=0} = 0. \end{aligned} \tag{10}$$

These boundary conditions may be extended by interpolating between the two extremes. In particular, Ambegaokar, de Gennes, and Rainer (AdGR) showed that diffuse scattering from an atomically rough surface leads to a GL boundary condition in which the transverse orbital components of the order parameter are finite at the surface, but extrapolate linearly to zero a distance $b_T = 0.54\xi_0$ past the boundary. Thus, we introduce more general boundary conditions defined by

$$\begin{aligned} A_{\alpha z} \Big|_{z=0} &= 0, \\ \nabla_z A_{\alpha x} \Big|_{z=0} &= \frac{1}{b_T} A_{\alpha x} \Big|_{z=0} \\ \nabla_z A_{\alpha y} \Big|_{z=0} &= \frac{1}{b_T} A_{\alpha y} \Big|_{z=0}, \end{aligned} \tag{11}$$

where $b_T = b'_T \xi_0$ is the extrapolation length. The parameter b'_T is allowed to vary from $b'_T = 0$, maximal pairbreaking, to $b'_T \rightarrow \infty$, minimal pairbreaking. The film geometry consists of two infinite coplanar surfaces separated by a distance D with

³He filling the region between them. The boundary conditions in Eq. 11 are imposed at $z = \pm D/2$.

2.4 Extrapolating GL Theory to Low Temperatures

GL theory is only expected to be accurate in the vicinity of T_c . This is easily seen in the order parameter amplitude, $\Delta^2 \sim 1 - T/T_c$, which varies linearly in T down to $T = 0$, whereas the weak-coupling BCS order parameter saturates at low temperatures. In confined ³He, this difference is reflected in the characteristic length scale for variations of the order parameter, which in GL theory is

$$\xi_{GL}(T) = \left[\frac{7\zeta(3)/20}{1 - T/T_c} \right]^{1/2} \left(\frac{\hbar v_f}{2\pi k_B T_c} \right). \tag{12}$$

In weak-coupling BCS theory, the characteristic length scale is

$$\xi_{\Delta}(T) = \frac{\hbar v_f}{\sqrt{10}\Delta_B^{BCS}(T)}, \tag{13}$$

which is significantly larger than $\xi_{GL}(T)$ at low temperatures. In order to more accurately extrapolate the spatial variations of the order parameter, as well as the confinement phase diagram, to lower temperatures, we rescale the film of thickness in the GL equations $D \rightarrow D(T)$ with

$$D(T) = D(T_c) \frac{\xi_{GL}(T)}{\xi_{\Delta}(T)}, \tag{14}$$

where $D(T_c) = D$ is the thickness of the film and $D(T)$ is a rescaled thickness used within the GL theory calculation. Figure 3 shows the effect of this rescaling on the weak-coupling GL theory phase diagram for the region of stability of the Stripe phase in comparison to the Stripe phase region obtained in weak-coupling quasiclassical theory [1]. Rescaling lengths in the GL theory in terms of $\xi_{\Delta}(T)$ gives a more accurate representation of the confinement phase diagram than simple extrapolation of the GL results to low temperature. The deviations that remain reflect the non-locality of the quasiclassical theory for inhomogeneous phases for $T \ll T_c$.

3 Stripe Phase

The Stripe phase spontaneously breaks translational symmetry in the plane of the film. We assume it does so along the x axis, leaving the order parameter translationally invariant along the y direction. Broken translational symmetry leads to a new length scale, L , which is the half-period of the Stripe phase order parameter; L is an emergent length scale, which varies with temperature, pressure, film thickness, and the surface boundary condition, and must be determined by numerical minimization of the GL free energy in parallel with the self-consistent determination of the order parameter.

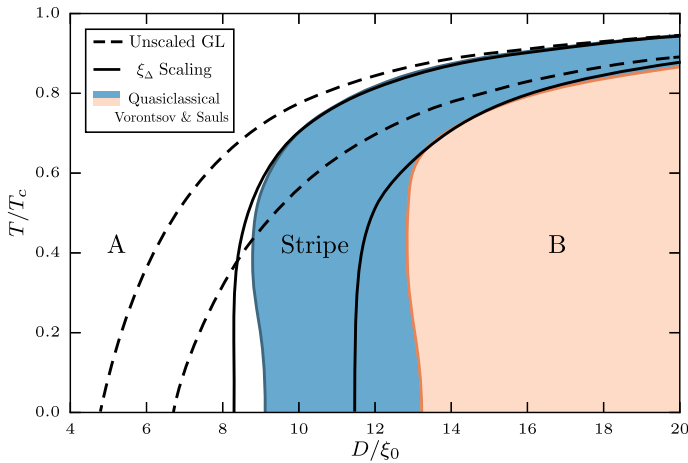


Fig. 3 Comparison of the phase diagrams calculated within weak-coupling quasiclassical theory (blue and orange lines), weak-coupling GL theory (dashed lines), and weak-coupling GL theory with D rescaled by $\xi_{GL}(T)/\xi_{\Delta}(T)$ (solid black lines) (Color figure online)

3.1 Order Parameter

The Stripe phase is predicted to be stable in superfluid ^3He films of thickness $D \sim 10\xi_0$ [1]. In weak-coupling theory, this phase appears as a second-order transition between the Planar and B phases, and for $D \lesssim D_{c2} \approx 13\xi_0$, corresponds to a periodic array of degenerate B phase domains separated by domain walls [1].

For broken translational symmetry along the x axis the residual symmetry of the Stripe phase is defined by the point group,

$$H = \left\{ e, c_{2x}^L c_{2x}^S \right\} \times \left\{ e, \pi_{xy}^L \pi_{xy}^S \right\} \times \left\{ e, \pi_{xz}^L \pi_{xz}^S \right\} \times \left\{ e, e^{i\pi} c_{2z}^L \right\} \times T, \tag{15}$$

where c_{2x}^L is an orbital space π rotation about the x axis, π_{xz}^S is a spin space reflection about the xz plane, and T is the operation of time reversal. Based on this residual symmetry group, we can simplify the form of the order parameter for the Stripe phase to

$$A(x, z) = \begin{pmatrix} A_{xx} & 0 & A_{xz} \\ 0 & A_{yy} & 0 \\ A_{zx} & 0 & A_{zz} \end{pmatrix}, \tag{16}$$

where the remaining five components are functions of x and z , and are all real due to time reversal symmetry.

The spatial dependences of the self-consistent order parameter components for the Stripe phase at pressure $p = 3$ bar, $T/T_c = 0.5$, thickness $D = 12\xi_0$ with specular surfaces are shown in Fig. 4. Note that the calculated half-period is $L \approx 23.6\xi_0$, and that the dominant components are the diagonal elements, A_{xx} , A_{yy} , and A_{zz} . The latter exhibits a domain wall separating degenerate B-like order parameters with $\text{sgn}(A_{zz}) = \pm 1$. The pairbreaking of A_{zz} on the boundaries is alleviated by the large

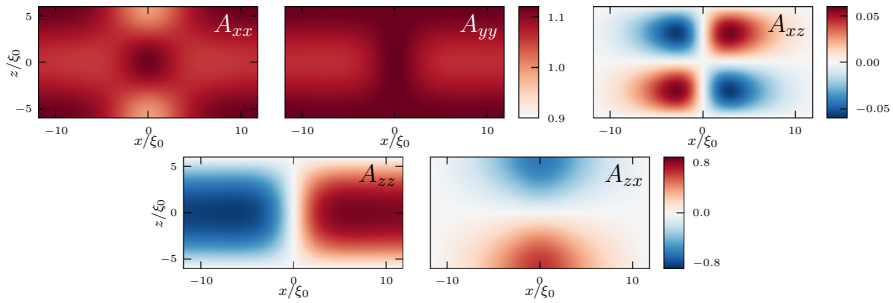


Fig. 4 Stripe phase order parameter for specular surfaces as functions x and z for $D = 12\xi_0$, $p = 3$ bar, $T = 0.5T_c$, and calculated period $L \approx 23.6\xi_0$. The amplitudes are scaled in units of the bulk B phase order parameter, $\Delta_B = \sqrt{|\alpha(T)|/6(\beta_{12} + 1/3\beta_{345})}$ (Color figure online)

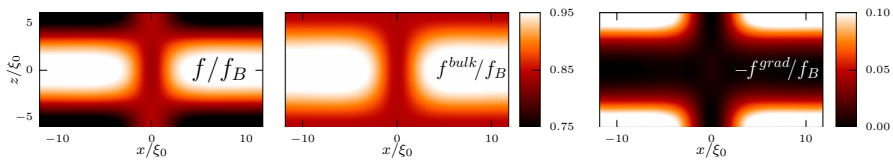


Fig. 5 Energy density of the Stripe phase with specular surfaces for $D = 12\xi_0$, $p = 3$ bar, $T = 0.5T_c$, and calculated period $L \approx 23.6\xi_0$. The energy density f is scaled by the unconfined bulk energy density $f_B = \frac{1}{2}\alpha(T) \Delta_B(T)^2 < 0$, and is also shown separated into bulk and gradient contributions (Color figure online)

off-diagonal component, A_{zx} , at the junction with the domain wall. The remaining symmetry allowed amplitude, A_{xz} , clearly exhibits the symmetry with respect to C_{2x}^L, C_{2x}^S , but is smaller by an order of magnitude.

The stability of the Stripe phase results from a tradeoff between the lowering of the energy at junctions where the surfaces intersect the domain wall (note the gradient energy in Fig. 5) and the cost in energy, away from the film surface, due to the suppression of the order parameter along the domain wall. The total condensation energy density, with separate bulk and gradient energy densities, is shown in Fig. 5.

3.2 Variational Model

The magnitude of the half-period of the Stripe phase, L , is most easily determined using a variational form of the order parameter; L is a minimum at the Stripe–Planar transition and diverges at the Stripe–B transition. At the Stripe–Planar transition, and for specular boundaries, L may be derived from the variational order parameter,

$$A(x, z) = \begin{pmatrix} \Delta_{xx} & 0 & 0 \\ 0 & \Delta_{yy} & 0 \\ A_{zx} & 0 & A_{zz} \end{pmatrix}, \tag{17}$$

where $A_{zx} = -\Delta_{zx} \cos(\pi x/L) \sin(\pi z/D)$ and $A_{zz} = \Delta_{zz} \sin(\pi x/L) \cos(\pi z/D)$. At the Stripe–Planar transition, we assume that

$$\Delta_{yy} = \Delta_{xx}, \quad \Delta_{zx} \ll \Delta_{xx}, \quad \text{and} \quad \Delta_{zz} \ll \Delta_{xx}. \quad (18)$$

After spatially averaging and dropping terms greater than second order in Δ_{zx} and Δ_{zz} the resulting GL functional reduces to,

$$\begin{aligned} F_{\text{var}} = & 2\alpha\Delta_{xx}^2 + 4\beta_P\Delta_{xx}^4 - \frac{\pi^2 K_{23}\Delta_{zx}\Delta_{zz}}{2DL} \\ & + \Delta_{zx}^2 \left\{ \frac{\alpha}{4} + \beta_P\Delta_{xx}^2 + \pi^2 \left(\frac{K_{123}D^2 + K_1L^2}{4D^2L^2} \right) \right\} \\ & + \Delta_{zz}^2 \left\{ \frac{\alpha}{4} + \beta_{12}\Delta_{xx}^2 + \pi^2 \left(\frac{K_1D^2 + K_{123}L^2}{4D^2L^2} \right) \right\}, \end{aligned} \quad (19)$$

where $\beta_{ijk\dots} = \beta_i + \beta_j + \beta_k + \dots$, $K_{ijk\dots} = K_i + K_j + K_k + \dots$, and $\beta_P = \beta_{12} + 1/2\beta_{345}$ determine bulk free energy of the Planar phase. Minimizing F_{var} with respect to Δ_{xx}^2 gives,

$$\Delta_{xx}^2 = \frac{|\alpha|}{2\beta_P} - \frac{\Delta_{zx}^2}{8} - \frac{\Delta_{zz}^2\beta_{12}}{8\beta_P}. \quad (20)$$

The reduced free energy functional then simplifies to

$$\begin{aligned} F_{\text{var}} = & -\frac{\alpha^2}{4\beta_P} - \frac{\pi^2 K_{23}\Delta_{zx}\Delta_{zz}}{2DL} \\ & + \Delta_{zx}^2 \left\{ \pi^2 \left(\frac{K_{123}D^2 + K_1L^2}{4D^2L^2} \right) \right\} \\ & + \Delta_{zz}^2 \left\{ \alpha \left(\frac{\beta_P - \beta_{12}}{4\beta_P} \right) + \pi^2 \left(\frac{K_1D^2 + K_{123}L^2}{4D^2L^2} \right) \right\}. \end{aligned} \quad (21)$$

The last three terms in Eq. 21 determine when non-zero values of Δ_{zx} and Δ_{zz} are favorable and the Stripe–Planar instability occurs. At the instability

$$\begin{aligned} \alpha(T) = & -\frac{\pi^2\beta_P}{D^2L^2(\beta_P - \beta_{12})} \left\{ -2DLK_{23} \left(\frac{\Delta_{zx}}{\Delta_{zz}} \right) \right. \\ & \left. + \left(D^2K_{123} + L^2K_1 \right) \left(\frac{\Delta_{zx}}{\Delta_{zz}} \right)^2 + \left(D^2K_1 + L^2K_{123} \right) \right\}. \end{aligned} \quad (22)$$

Minimizing F_{var} with respect to the ratio Δ_{zx}/Δ_{zz} gives

$$\frac{\Delta_{zx}}{\Delta_{zz}} = \frac{DLK_{23}}{D^2K_{123} + L^2K_1}. \quad (23)$$

Combining Eq. 23 with Eq. 22 yields the Planar–Stripe instability temperature, T_{PS} , as a function of D and L . Optimizing T_{PS} with respect to the Stripe phase period yields,

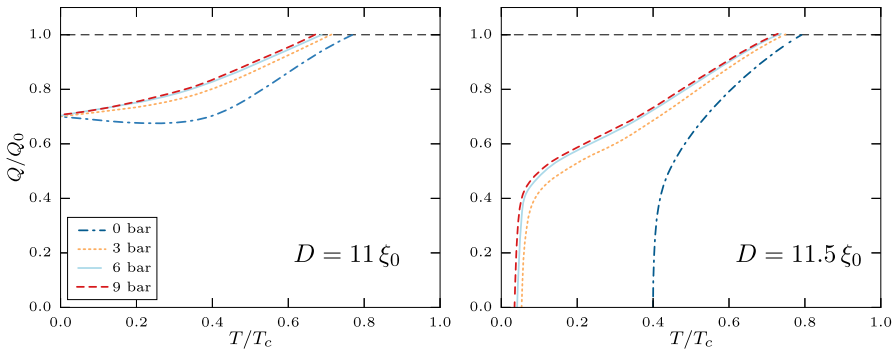


Fig. 6 Temperature and pressure dependence of the wavenumber Q for film thicknesses $D = 11 \xi_0$, with no Stripe to B transition (*left panel*), and $D = 11.5 \xi_0$, with a Stripe to B transition (*right panel*). The onset of the Stripe transition is based on the Planar–Stripe instability, i.e., omitting the A phase (Color figure online)

$$L = \sqrt{\frac{K_{123}}{|K_{23} - K_1|}} D, \tag{24}$$

which for weak-coupling values of K_1 , K_2 , and K_3 , reduces to $L = \sqrt{3}D$.

Although the Planar to Stripe transition is interrupted by a first-order transition to the A phase, the Stripe–Planar instability determines the scale of the half-period, L , and the temperature region where the Stripe phase is expected to be stable. The half-period defines the wavenumber, $Q_0 = \pi/\sqrt{3}D$, of the single-mode instability at T_{PS} . The wavenumber varies with the film thickness, D , and temperature. Figure 6 shows the temperature dependence of Q for two values of the film thickness starting from the Planar to Stripe instability at T_{PS} , i.e., omitting the A phase. The stability of the A phase relative to the Planar phase changes the Stripe instability to a first-order transition at a lower temperature T_{AS} . For $D = 11 \xi_0$, the stable region of Stripe phase persists to $T = 0$, while for $D = 11.5 \xi_0$ there is a Stripe to B phase transition at a temperature, $T_{SB} < T_{PS}$. In both cases, the wavenumber decreases (L increases) as T drops below T_{PS} , with $Q \rightarrow 0$ ($L \rightarrow \infty$) as $T \rightarrow T_{SB}$. Strong-coupling corrections to the free energy lead to a modest increase the period of the Stripe phase away from the Stripe to B transition; however, the transition temperature, T_{SB} , is sensitive to pressure (strong-coupling) as shown in the right panel of Fig. 6.

4 Stripe Phase Stability

The most prominent effect of strong-coupling corrections to the weak-coupling BCS theory in bulk superfluid ^3He is the stability of the A phase above $p_{PCP} = 21.22$ bar. In sufficiently thin films, the A phase is energetically stable relative to the B phase even in weak-coupling theory, and is degenerate with the Planar phase [1, 14]. Strong-coupling corrections favor the A phase over the Planar phase, leading to a stable A phase in thin films at all pressures. Since the Stripe phase can be understood as a periodic array of

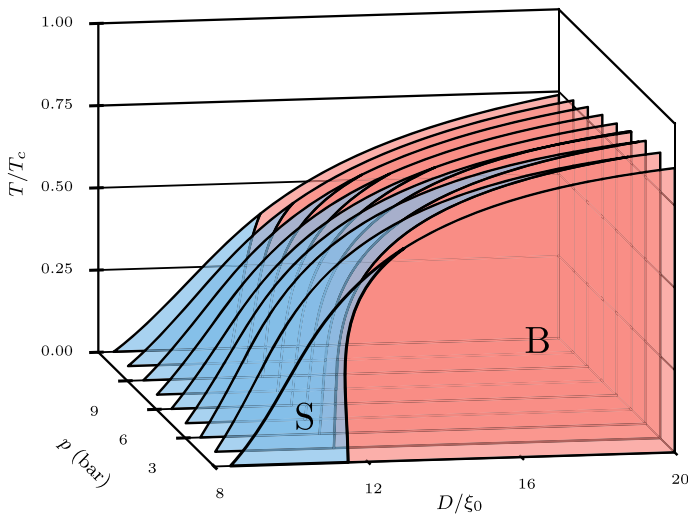


Fig. 7 Pressure–temperature–confinement phase diagram for the film with minimal pairbreaking boundaries and experimental strong-coupling corrections. The A phase is stable everywhere not excluded by the Stripe and B phases (Color figure online)

degenerate B phase domains separated by time-reversal invariant domain walls, one expects strong-coupling to favor the A phase near the Planar–Stripe instability line. Indeed, the A phase suppresses the Planar to Stripe instability temperature. However, the Stripe phase is found to be stable over a wide range of temperatures and pressures.

Figure 7 shows the phase diagram for minimal pairbreaking (specular) surfaces at pressures from 0 to 12 bar, with the Stripe phase onsetting at temperatures above $0.5T_c$. The accuracy of the strong-coupling GL theory is expected to diminish at very low temperatures; therefore, we show results for low and intermediate pressures for which the A- to Stripe transition onsets above $0.5T_c$. Note that at $T = 0$ the strong-coupling GL corrections vanish, and the phase boundaries are determined by weak-coupling theory at $T = 0$ and thus pressure independent. This is an artifact of the temperature scaling of the strong-coupling GL parameters. It is known that there are residual strong-coupling corrections at the few percent level in the limit $T = 0$ [15].

A striking difference between the two sets of strong-coupling β parameters shown in Figs. 1 and 2 is evident at low pressures. The $\Delta\beta_i^{sc}$ from Choi et al. [16] are non-monotonic between $p = 0$ and $p = 12$ bar, which leads to maximal stability of the Stripe phase at $p \approx 3$ bar. In contrast, the theoretically calculated strong-coupling corrections are monotonic functions of pressure and predict maximal stability of the Stripe phase at $p = 0$ bar and decreasing stability with increasing pressure.

4.1 Pressure–Temperature Phase Diagram

Although a number of experiments have been reported on superfluid ^3He in planar geometries, of particular interest are those involving slabs of thickness $D \approx 700$ nm and $D \approx 1080$ nm, which are in the range of confinement where the Stripe phase is

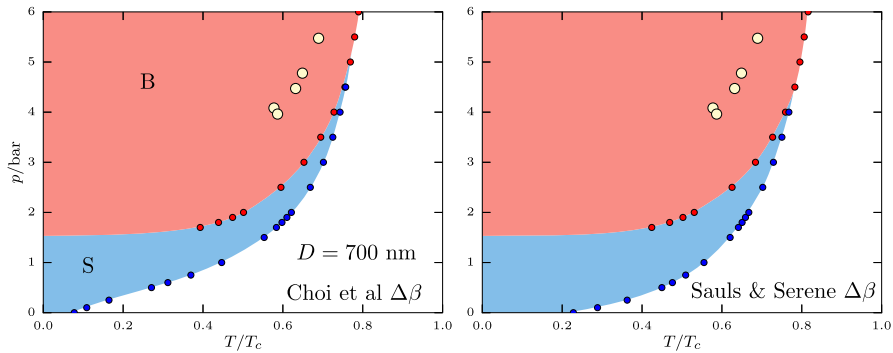


Fig. 8 Pressure–temperature phase diagram for a film of thickness $D = 700$ nm with minimal pairbreaking (specular) boundary conditions. The A phase is stable everywhere in the white region below the bulk transition temperature. The larger yellow circles are data for the A–B transition based on NMR from Levitin et al. obtained with ^4He preplating [2] (Color figure online)

expected to be stable. Levitin et al. [2] (RHUL group) used transverse NMR frequency shifts to determine transition temperatures in these cells. They did not find NMR evidence of the Stripe phase. These experiments were done both with and without preplating the surfaces of the slab with ^4He , the presence of which greatly increases the specularity of the surface. Without the ^4He present, the RHUL group reported large suppression of the onset of the superfluid transition—a suppression larger than that predicted theoretically for maximally pairbreaking retro-reflective surface scattering. The explanation or origin of this anomalous suppression is currently lacking. Thus, we focus on the measurements done with ^4He preplating, which exhibit minimal T_c suppression, and may be modeled theoretically with minimal pairbreaking boundary conditions (specular scattering).

Calculations of the phase diagram for $D = 700$ nm are shown in Fig. 8. The A phase onsets at the bulk T_c . There is an A- to Stripe transition followed by the Stripe to B transition. For both sets of strong-coupling β parameters, the Stripe phase is predicted to be stable at low pressures and at experimentally accessible temperatures. Although the stability of the A phase is maximal with specular boundary conditions, the calculated A–B or A–S phase transition occurs at significantly higher temperature than that reported by the RHUL group. The discrepancy is sufficiently large that it is well outside uncertainties in the magnitude of the strong-coupling parameters based bulk A- and B phase free energies. Based on our calculations accessing the Stripe phase would be optimal for pressures between $p = 1$ and $p = 1.5$ bar.

For the thicker slab geometry, $D = 1080$ nm, shown in Fig. 9, the Stripe phase is predicted to have a negligible region of stability in the pressure-temperature plane based on the β parameters from Choi et al. [16], and only a small window of stability at the lowest pressures based on the theoretically calculated strong-coupling parameters.

4.2 Effects of Surface Boundary Conditions on the Phase Diagram

We use the variable boundary conditions in Eq. 11 to investigate the sensitivity of the Stripe phase to surface disorder. Figure 10 shows the temperature-confinement

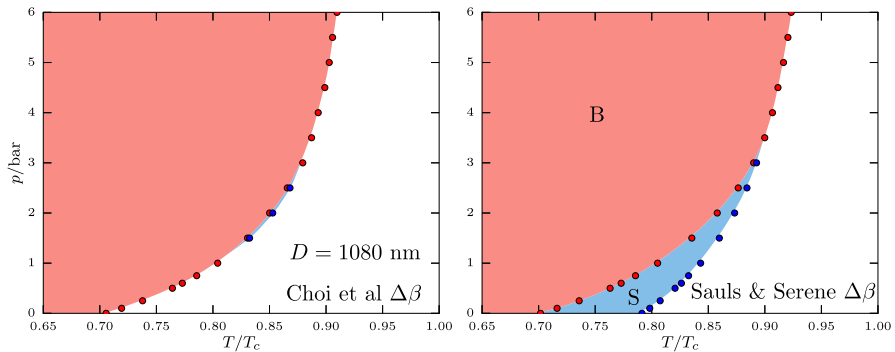


Fig. 9 Pressure–temperature phase diagram for a film of thickness $D = 1080$ nm with minimal pairbreaking boundaries. The A phase is stable everywhere not excluded by the Stripe and B phases (Color figure online)

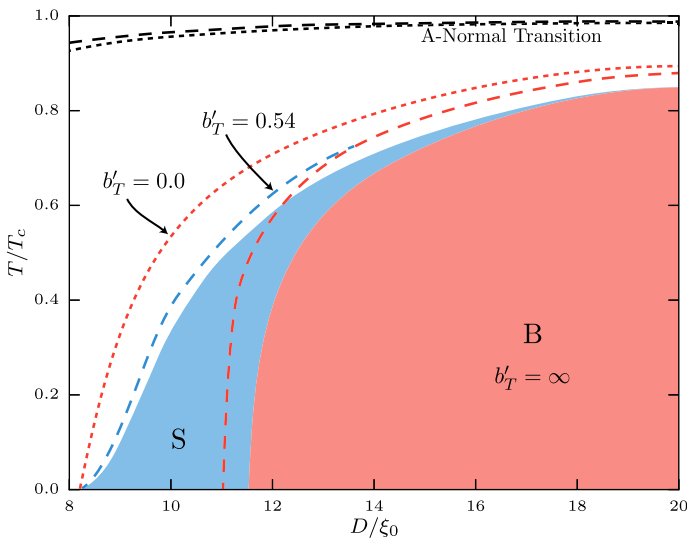


Fig. 10 Temperature–confinement phase diagram for films at $p = 3$ bar with the Choi et al. strong-coupling corrections. Results for three boundary conditions are shown: minimal pairbreaking, $b'_T \rightarrow \infty$ (solid); diffuse, $b'_T = 0.54$ (dashed); and maximal pairbreaking, $b'_T = 0$ (dotted). For diffuse and maximal pairbreaking, the suppression of the A to normal phase transitions is also shown (Color figure online)

phase diagram at $p = 3$ bar for maximal ($b'_T = 0$), diffuse ($b'_T = 0.54$), and minimal ($b'_T = \infty$) pairbreaking boundary conditions. Maximal stability of the Stripe phase occurs for minimal pairbreaking, i.e., specular surfaces, as shown by the blue region of stable Stripe phase. Note that for diffuse scattering the region of Stripe phase stability does not differ significantly from that for specular boundary scattering. Conversely, for maximal pairbreaking the Stripe phase exists only in the vicinity of $T = 0$.

5 NMR Signatures of the Stripe Phase

Nuclear magnetic resonance (NMR) spectroscopy of the ^3He order parameter is based on resonance frequency shifts originating from the Cooper pair contribution to the nuclear magnetic dipole energy, $\Delta\Omega_D = \int_V d^3r f_D[A]$, which evaluated to leading order in A is

$$f_D = g_D \left(|Tr A|^2 + Tr AA^* \right), \tag{25}$$

where $g_D = \frac{\chi}{2\gamma^2} \Omega_A^2 / \Delta_A^2$ is the nuclear dipole coupling; γ is the ^3He nuclear gyro-magnetic ratio; χ is the nuclear magnetic susceptibility of normal ^3He ; and Ω_A is the A phase longitudinal NMR resonance frequency. The dipole energy, of order $g_D \Delta_A^2$, lifts the degeneracy of relative rotations of the spin- and orbital state of the Cooper pairs.

NMR spectroscopy is based on the NMR frequency shift, $\Delta\omega = \omega - \omega_L$, resulting from the dipolar torque acting on the total nuclear magnetization. The shift depends in general on the orientation of the NMR field, \mathbf{H} , the initial tipping angle, β , generated by the r.f. pulse, and particularly the spin- and orbital structure of the order parameter. We use the reduction of Leggett’s theory of NMR in ^3He proposed by Fomin [17], valid for intermediate magnetic fields, $\Omega_A \ll \omega_L \ll \Delta$, where $\omega_L = \gamma H$ is the Larmor frequency [17]. The key approximation is the first inequality which provides a separation of “fast” and “slow” timescales for the spin dynamics. The second inequality allows us to neglect the deformation of the order parameter by the Zeeman field. Similarly, for inhomogeneous states we use the separation of length scales for spatial variations of the Stripe phase, of order $L \sim D \approx 1 \mu\text{m}$, both small compared to the dipole coherence length, $\xi_D \equiv \sqrt{g_D/K_1} \approx 20 \mu\text{m}$. The spin degrees of freedom of the order parameter cannot vary on length scales shorter than the dipole coherence length ξ_D . Thus, for $L \ll \xi_D$ the nuclear spin dynamics is determined by the spatially averaged dipole energy. An exception to this spatial averaging occurs near the Stripe-B transition where the period of the Stripe phase diverges. In this limit the dipolar energy varies on sufficiently long spatial scales that the spin dynamics is determined by a spatially varying dipolar potential. Combined with Fomin’s formulation, the separation in scales for spatial variations of the orbital and spin components of the order parameter allows us to calculate the non-linear NMR frequency shifts for the inhomogeneous phases of the thin film as described in Ref. [3].

5.1 Translationally Invariant Planar-Distorted B Phase

For non-equal-spin pairing (non-ESP) states, e.g., the polar distorted B phase or the Stripe phase, the nuclear magnetic susceptibility, χ , is suppressed relative to that of normal ^3He , χ_N . For all non-ESP phases, including the Stripe phase, the susceptibility can be expressed as

$$\chi_B = \frac{\chi_N}{1 + 2 g_z / \chi_N (\langle \Delta_{zx}^2 \rangle + \langle \Delta_{zz}^2 \rangle)}. \tag{26}$$

For a non-ESP superfluid phase of a ^3He film with the magnetic field $\mathbf{H}||\mathbf{z}$, for both the B and Stripe phases, there are two possible dipole orientations corresponding to different local minima in the dipole energy [18]. The first orientation is a minimum of the dipole energy and has positive frequency shift, which following Levitin et al. we denote as the B^+ state in the case of the translationally invariant B phase. The frequency shift for the B^+ state is obtained as

$$\omega\Delta\omega^+ = \frac{\gamma^2}{\chi_B} g_D \times \begin{cases} \frac{\langle A_{xx}^2 \rangle - \langle A_{xx} A_{zz} \rangle^2}{\langle A_{xx}^2 \rangle} + 2 \left(\frac{\langle A_{xx} A_{zz} \rangle^2}{\langle A_{xx}^2 \rangle} - \langle A_{zz}^2 \rangle \right) \cos \beta, & \cos \beta \geq \cos \beta^*, \\ -\langle A_{xx}^2 \rangle - \langle A_{xx} A_{zz} \rangle - 2 \langle (A_{xx} + A_{zz})^2 \rangle \cos \beta, & \cos \beta < \cos \beta^*, \end{cases} \quad (27)$$

where $\langle \dots \rangle = (1/V) \int_V d^3R \dots$ denotes spatial averaging, and

$$\cos \beta^* = \frac{1}{2} \left(\frac{\langle A_{xx} A_{zz} \rangle - 2 \langle A_{xx}^2 \rangle}{\langle A_{xx} A_{zz} \rangle + \langle A_{xx}^2 \rangle} \right) \quad (28)$$

is the critical angle [19].

Axial symmetry of the Planar-distorted B phase implies $\langle A_{yy}^2 \rangle = \langle A_{xx}^2 \rangle$; thus, only $\langle A_{xx}^2 \rangle$, $\langle A_{zz}^2 \rangle$, and $\langle A_{xx} A_{zz} \rangle$ are non-zero. This NMR resonance is analogous to the Brinkman–Smith mode in bulk ^3He –B, but with a positive frequency shift at small tipping angle and a shifted critical angle. The translationally invariant, but metastable, B_- state corresponds to a minimum of the combined dipole and Zeeman energies, and has a frequency shift given by [19]

$$\omega\Delta\omega^- = \frac{\gamma^2}{\chi_B} g_D \left\{ - \left(\langle A_{xx}^2 \rangle + 2 \langle A_{zz}^2 \rangle \right) \cos \beta \right\}. \quad (29)$$

This mode has a negative frequency shift at small tipping angles and, unlike the B_+ state, has no critical angle, and therefore no deviation from cosine tipping angle dependence. This state is metastable in the high-field limit, but unstable when the Zeeman energy is comparable to the dipole energy. (See also Ref. [20].) The tipping angle dependences of both Planar-distorted B phase states are shown in Fig. 11 plotted as a function of $\cos \beta$. The positive (negative) shift at small tipping angle is the signature of the B^+ (B^-) state in the NMR spectra of the RHUL group [2]. These identifications are confirmed by non-linear NMR measurements [19] showing both the pure cosine tipping angle dependence of $\omega\Delta\omega$ for the B^- state, and the “kink” in the shift at the critical angle β^* for the B^+ state. Note that for $D = 12\xi_0$ at $p = 3$ bar there is a small slope to the positive shift for $\cos \beta > \cos \beta^*$.

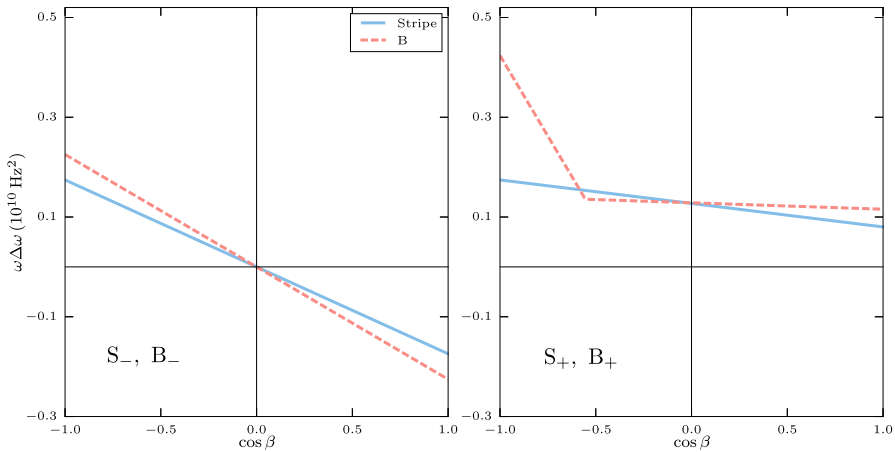


Fig. 11 Transverse NMR frequency shifts as a function of tipping angle β at $D = 12\xi_0$, $p = 3$ bar, and $T = 0.5 T_C$, with minimal pairbreking for the B^\pm and S^\pm states (Color figure online)

5.2 Non-linear NMR Shifts for the S^\pm Stripe Phases

The breaking of both translational and rotational symmetry in the plane of the film by the Stripe phase leads to a qualitatively different transverse NMR frequency shift for the Stripe phase with relative spin–orbit rotation corresponding to a minimum of the dipole energy, i.e., the S^+ state,

$$\omega\Delta\omega^+ = \frac{1}{2} \frac{\gamma^2}{\chi_B} g_D \left\{ \left\langle (A_{yy} + A_{xx})^2 \right\rangle - \left[\left\langle (A_{yy} - A_{xx})^2 \right\rangle + 8 \left\langle A_{zz}^2 \right\rangle - 4 \left(\left\langle A_{xz}^2 \right\rangle + \left\langle A_{zx}^2 \right\rangle \right) \right] \cos \beta \right\}. \quad (30)$$

The S^+ phase is distinguished with respect to both the bulk B phase and the Planar-distorted B^+ phase by the absence of a critical tipping angle. This results from spatial averaging over the period of the Stripe phase which contains equal volumes of $A_{zz} > 0$ and $A_{zz} < 0$ giving $\langle A_{xx} A_{zz} \rangle = \langle A_{yy} A_{zz} \rangle = 0$.

By contrast the frequency shift of the metastable S^- phase does not differ substantially from that of the B^- phase,

$$\omega\Delta\omega^- = \frac{1}{2} \frac{\gamma^2}{\chi_B} g_D \left\{ \left\langle (A_{yy} - A_{xx})^2 \right\rangle (1 + \cos \beta) - \left[2 \left\langle A_{xx}^2 \right\rangle + 2 \left\langle A_{yy}^2 \right\rangle + 8 \left\langle A_{zz}^2 \right\rangle - 4 \left(\left\langle A_{xz}^2 \right\rangle + \left\langle A_{zx}^2 \right\rangle \right) \right] \cos \beta \right\}. \quad (31)$$

Note that the constant term in the shift for the S^- state proportional to the average $\langle (A_{yy} - A_{xx})^2 \rangle$ is absent for the B^- state; however, this constant shift is negligibly small. Figure 11 shows the comparison between the translationally invariant B^\pm NMR

shifts and those for the corresponding stable and metastable S^\pm Stripe phases. The primary NMR signature of the Stripe phase is the positive shift with an offset, a finite slope and the absence of critical angle. This signature clearly differentiates the S^+ phase from the B^\pm states and the A phase.

6 Summary and Outlook

By formulating a GL theory that incorporates pressure and temperature-dependent strong-coupling corrections, combined with temperature-dependent rescaling of the confinement length, D , we have greatly expanded the region of applicability of GL theory for calculations of the properties of confined superfluid ^3He . Strong-coupling corrections expand the region of stability of the A phase and decrease the region of stability of the Stripe phase; however, the Stripe phase remains stable in a large region of pressure, temperature, and confinement. The stability of the Stripe phase is insensitive to diffuse surface scattering; the phase diagram for specular and fully diffusive scattering predicts the Stripe phase to occur in nearly equivalent regions of the phase diagram. Non-linear NMR measurements are probably the best means of detecting the Stripe phase. The NMR signatures—positive shift with no critical angle—differentiate the S^+ phase from the B^\pm and A phases.

Acknowledgments The research of JJW and JAS was supported by the National Science Foundation (Grants DMR-1106315 and DMR-1508730).

References

1. A.B. Vorontsov, J.A. Sauls, Phys. Rev. Lett. **98**(4), 045301 (2007)
2. L.V. Levitin, R.G. Bennett, A. Casey, B. Cowan, J. Saunders, D. Drung, T. Schurig, J.M. Parpia, Science **340**(6134), 841 (2013)
3. J.J. Wiman, J.A. Sauls, Phys. Rev. B **92**(14), 144515 (2015)
4. K. Aoyama, Phys. Rev. B **89**, 140502 (2014)
5. V.V. Dmitriev, A.A. Senin, A.A. Soldatov, A.N. Yudin, Phys. Rev. Lett. **115**, 165304 (2015)
6. S. Autti, V.V. Dmitriev, V.B. Eltsov, J. Makinen, G.E. Volovik, A.N. Yudin, V.V. Zavjalov, **1** (2015), [arXiv:1508.02197](https://arxiv.org/abs/1508.02197)
7. J.I.A. Li, A.M. Zimmerman, J. Pollanen, C.A. Collett, W.P. Halperin, Phys. Rev. Lett. **114**, 105302 (2015)
8. D. Rainer, J.W. Serene, Phys. Rev. B **13**, 4745 (1976)
9. H. Choi, J.P. Davis, J. Pollanen, T. Haard, W. Halperin, Phys. Rev. B **75**(17), 174503 (2007)
10. E. Thuneberg, Phys. Rev. B **36**, 3583 (1987)
11. J.A. Sauls, J.W. Serene, Phys. Rev. B **24**, 183 (1981)
12. J.A. Sauls, Phys. Rev. B **84**, 214509 (2011)
13. V. Ambegaokar, P. de Gennes, D. Rainer, Phys. Rev. A **9**, 2676 (1975)
14. A. Vorontsov, J.A. Sauls, Phys. Rev. B **68**, 064508 (2003)
15. J.W. Serene, D. Rainer, Phys. Rep. **101**, 221 (1983)
16. H.C. Choi, A.J. Gray, C.L. Vicente, J.S. Xia, G. Gervais, W.P. Halperin, N. Mulders, Y. Lee, Phys. Rev. Lett. **93**(14), 145302 (2004)
17. I. Fomin, J. Low Temp. Phys. **31**(3–4), 509 (1978)
18. Y.M. Bunkov, G.E. Volovik, Eur. Phys. Lett. **21**(8), 837 (1993)
19. L.V. Levitin, R.G. Bennett, E.V. Surovtsev, J.M. Parpia, B. Cowan, A.J. Casey, J. Saunders, Phys. Rev. Lett. **111**, 235304 (2013)
20. L. Levitin, Experimental Studies of the Superfluid Phases of Confined ^3He . Ph.D. thesis, Egham, UK (2012)